Article:
Zhang, X, Ries, ME orcid.org/0000-0002-8050-3200 and Hine, PJ (2021) Time–Temperature Superposition of the Dissolution of Silk Fibers in the Ionic Liquid 1-Ethyl-3-methylimidazolium Acetate. Biomacromolecules, 22 (3). pp. 1027-1324. ISSN 1525-7797

https://doi.org/10.1021/acs.biomac.0c01467

Time-temperature superposition of the dissolution of silk fibres in the ionic liquid 1-ethyl-3-methylimidazolium acetate

Xin Zhang, Michael E. Ries, Peter J. Hine*

Soft Matter Physics Research Group, School of Physics and Astronomy, University of Leeds, Leeds, LS2 9JT, United Kingdom

ABSTRACT

This study investigated the dissolution of silk multifilament fibres in the ionic liquid 1-ethyl-3-methylimidazolium acetate. The dissolution process was found to create a silk composite fibre, comprising undissolved silk multi-filaments surrounded by a coagulated silk matrix. The dissolution procedure was carried out for a range of temperatures and times. The resulting composite fibres were studied using a combination of optical microscopy, wide angle X-ray diffraction (XRD) and tensile testing. An azimuthal (alpha) XRD scan enabled the orientation of the composite silk filaments to be quantified through a 2nd Legendre Polynomial function (P_2). The P_2 results could be shifted to construct a single master curve using time-temperature superposition (TTS). The shifting factors were found to have an Arrhenius behaviour with an

activation energy of 138 ± 13 kJ/mol. Using a simple rule of mixtures the P_2 measurements were used to calculate the dissolved silk matrix volume fraction (V_m), which also displayed TTS forming a single master curve with an activation energy 139 ± 15 kJ/ mol. The tensile Young's Modulus of each silk composite filament was measured and these results similarly formed a master curve with an activation energy of 116 ± 12 kJ/mol.

KEYWORDS

silk

dissolution

time-temperature superposition

activation energy

1. INTRODUCTION

Natural fibres (both plant and animal based) have become a popular choice for the reinforcing phase of composites, as a replacement for non-degradable petroleum based fibres.[1-3] Among animal fibres, silk fibres have attracted a lot of interest, due to a combination of controllable biodegradation, superior biocompatibility and remarkable mechanical properties.[4-7] Mulberry silk obtained from a silkworm, also named Bombyx mori silk, has been used for textile production for centuries, and in biomedical sutures for decades.[8, 9] Due to the successful use of B. mori silk as suture material, silk has been further extended to various innovative applications, including biomaterials for drug delivery and tissue engineering.[10-12] Regenerated silk solutions also have been used to form a variety of biomaterials for medical applications, such as gels, sponges and

films.[13-15] To discover the full potential of silk fibres for enormous applications, fundamental knowledge with physics, chemistry and biology concepts are highly required.

Bombyx mori silk, consists of microfilaments approximately 5-10 μm in diameter. A single Bombyx mori silk fibre contains two fibrous core proteins named silk fibroin (SF), and a protective glue-like coating named sericin that surround the SF threads.[16, 17] SF possesses a highly repetitive amino acid sequence and amorphous random coils that account for its excellent mechanical characteristics. However, extensive intra- and inter- molecular hydrogen bonds between the amino acids, disulfide bonds and the hydrophobic nature of the crystalline regions give it low solubility in alkali, dilute acid and common organic solvents.[10, 18, 19]

Ionic liquids (IL) represent a unique class of solvents that possess remarkable versatility and tunability.[20, 21] The extremely low melting points, low or zero vapour pressure, high thermal stability and easily altered structure[22], makes ionic liquids a popular solvent to dissolve some high crystallinity natural materials, i.e. lignocellulosic[23, 24] and protein-based natural materials.[25] Imidazolium-based ILs were firstly investigated as a 'green solvent' to dissolve cellulose by Swatloski et al. in 2002.[26] The dissolution of silk using ILs was subsequently studied by Philips et al. in 2004.[27] The results showed that the solubility of silk fibres in ILs can be manipulated by selecting different combinations of cations and anions. It has been found that anions (mainly halogens or small carboxylates) with strong hydrogen bond acceptors, such as Cl^-, $[Ac]^-$, and $[NO3]^-$, can disrupt the hydrogen bonds in the crystalline domains of silk fibres.[28-30] After dissolution, the SF protein mainly exists in random coils and α-helices. This water-soluble structure can be gradually transformed into a water-insoluble structure by soaking in polar organic

solvents, and subsequently manipulated to form films, membranes, hydrogels and fibrous materials. Therefore, the rinse treatment, or coagulation bath, has also been reported as a crucial step for the conformational character of the coagulated SF.[27, 31, 32] However, only a few studies have focused on characterising single silk fibre dissolution in an IL.[33]

In this work, a fundamental study of the dissolution mechanism of single silk fibres in an ionic liquid is reported. We have developed a novel approach to measure the volume fraction of the dissolved and then coagulated silk fraction, which we term the matrix fraction V_m of the obtained single all silk composites (ASC). This has been achieved by following the change in the average crystalline orientation of the ASC by measuring the 2nd Legendre Polynomial function (P_2) obtained from an azimuthal XRD scan. To our knowledge, this is the first time that the method of following P_2 has been used to determine the dissolution activation energy for silk fibres. The basis of this approach is that the dissolved and subsequently coagulated silk matrix reforms with a random crystalline orientation. Therefore, as the fraction of the coagulated silk (V_m) increases, the average crystalline orientation in the composite reduces. We report here, for the first time, how the dissolution of silk fibres depends on both time and temperature and most importantly, that a dissolution master curve can be formed using time-temperature superposition (TTS) to determine the corresponding dissolution activation energy (E_a). Mechanical measurements (Young's modulus) of the silk composites fibres were carried out, and these results also obey TTS yielding another estimate of the activation energy.

2. MATERIALS AND METHODS

2.1 Materials

Degummed bombyx mori silk fibre yarn (where the outer sericin layer has been removed) was purchased online (Mulberry Undyed Spun Silk from Airedale Yarns, UK) and stored under dry conditions in order to minimize the uptake of moisture from the surrounding atmosphere before use. One silk fibre thread consists of a few hundred individual silk filaments, each with a density of 1.361 g/cm^3 at 25°C.[34] The ionic liquid 1-ethyl-3-methylimidazolium acetate [C2mim][OAc] was purchased from Sigma-Aldrich, with a purification 97 %. Methanol was used as the regeneration bath because it has been reported to yield a high degree of crystallinity in the coagulated silk phase.[27]

2.2 Fabrication of single all silk composites(ASCs)

Single silk fibre threads were placed in the longitudinal direction and then fixed at both ends in an 8 x 8 cm^2 poly(tetrafluoroethylene) (Teflon) frame. A Teflon dish was filled with excess [C2mim][OAc] and placed in a vacuum oven (Shellab 17L Digital Vacuum Oven SQ-15VAC-16, Sheldon Manufacturing, Inc., USA) for 1 h, to carry out a pre-heating process before the dissolution experiments began. Then, the frame with the fibre threads was completely immersed into the preheated IL bath in the vacuum oven, for various dissolution times, at temperatures of 30, 35, 40 or 50°C (see Figure 1a) under vacuum.

When each procedure was finished, the partially dissolved silk fibre threads were removed from the IL bath and then soaked in a methanol (MeOH) bath for coagulation, as shown in Figure 1b, and the used [C2mim][OAc] was collected to be recycled. The coagulated ASCs were then washed in methanol for two days changing the medium twice. Finally, a one hour drying process with fibres left on the frame to stop shrinkage, in the vacuum oven at 100°C was applied (Figure 1c).

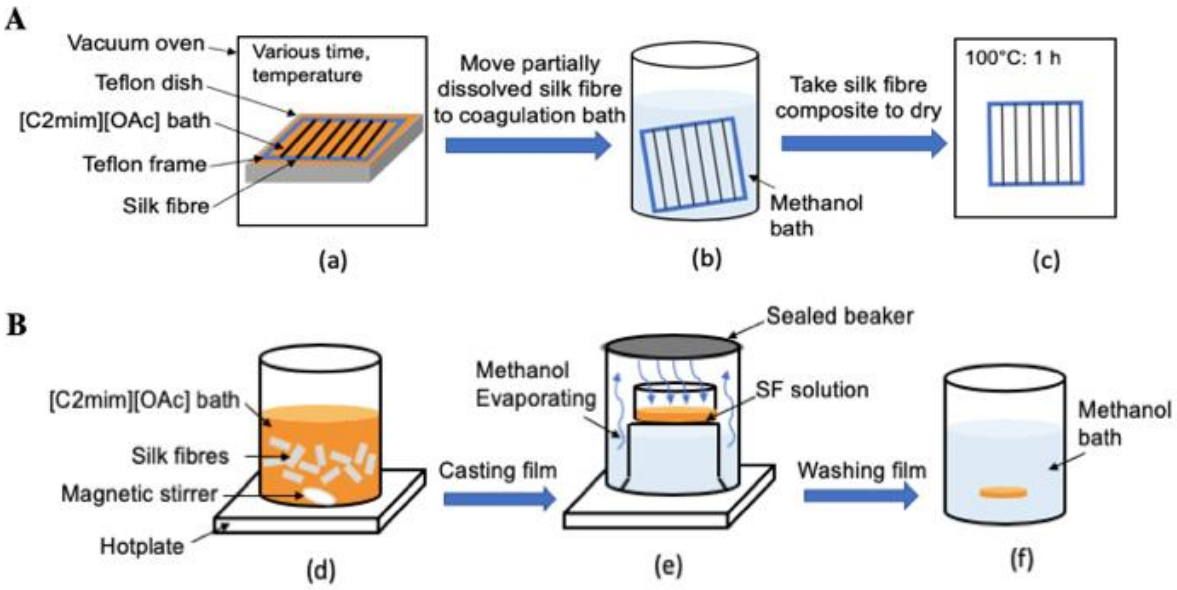

Figure 1 Diagram to show the (A) silk fibre composite fabrication process, starting from (a) dissolution, then (b) coagulation, (c) then finally drying in vacuum oven. (B) The film casting process, (d) dissolve silk fibres threads in [C2mim][OAc] solution, (e) controlled coagulation of the film using evaporated methanol, (f) washing the film in a methanol bath.

2.3 Preparation of silk fibroin (SF) solution and a coagulated silk film (CSF)

The degummed bombyx mori silk fibre was first dried in a vacuum oven set at a temperature of 65 °C for 24 hours and was then dissolved in [C2mim][OAc] solution with a magnetic stirrer, for 24 hours at 100 °C, at a speed of 80 rpm, as shown on Figure 1d. An amber coloured 10 % (w/v) SF solution was then obtained, which was then cast into a 5 cm x 5 cm polystyrene petri dish placed on a upside down beaker, and put into a larger scale beaker filled with methanol. The beaker was sealed and placed on a hotplate, allowing the methanol to slowly evaporate overnight inside the beaker, at 60 °C, and give controlled coagulation (Figure 1e). The cast film was then washed

with methanol statically for 2 days (Figure 1f), changing the medium twice, and then finally dried in a vacuum oven at 100 °C for one hour. The resulting film showed a light white colour with thickness of ~40 μm, and was termed the coagulated silk film (CSF). This film is considered representative of the matrix phase of the silk fibre composites.

2.4 Structure and morphology characterizations

The microstructures of both the raw single silk fibres and the partially dissolved (composite) fibres were imaged in cross section using an optical microscope (BH2-UMA, Olympus Corporation, Japan) in reflection. To obtain the cross-section image, single fibres were embedded in a slow cure epoxy resin (EpoxiCure 2, BUEHLER), and allowed to harden for 3 hours at 50 °C in an oven. After fully curing, the surface was ground and polished revealing the silk composite fibre cross sections. A representation schematic image of the embedded fibres is shown below in Figure 2.

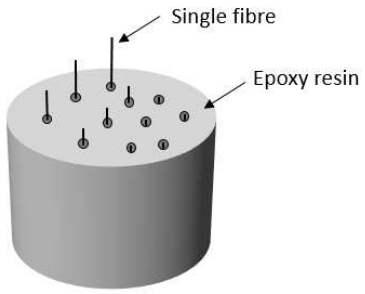

Figure 2 Schematic representation of single fibre threads embedded in epoxy resin, ready for taking the cross-sectional microscope images.

2.5 Wide-angle XRD characterization

X-ray studies of the crystallinity and crystal orientation of the silk composites and the coagulated silk film were performed at room temperature, using Cu Kα radiation (λ = 1.54 Å) at 40 kV and 30 mA (DRONEK 4-AXES, Huber Diffractionstechnik GmbH & Co. KG, Germany). The ASCs were mounted vertically on the goniometer and secured in position using Kapton tape. The diffraction intensity data was collected in transmission mode. For an equatorial (2θ scan), XRD data was collected from 2θ = 5 – 40°, at a scanning rate of 0.3 °/min, and a 2θ step of 0.2°.

For an azimuthal scan, an angle was chosen where the maximum crystalline intensity from the 2θ scan was found (20.6° for raw silk fibre) and 2θ was then kept fixed. The intensity distribution was then collected by varying the azimuthal angle from - 90° to 90° (0° = vertical), and a scanning rate of 2 °/min. 2D XRD photographs (Figure S1) showed that the raw silk fibre was characterised by a series of strong diffraction spots, whereas the coagulated film showed a series of rings. This indicates that the dissolution and coagulation process transforms the aligned crystal structure of the raw silk fibres into a randomly arranged crystal structure of the matrix. Our proposal is that the fraction of dissolved silk can therefore be determined by measuring the average orientation of each silk composite fibre, along with the values for the raw silk fibre and the coagulated film. Accordingly, the average orientation can be determined from the experimentally measured intensity distribution of the corresponding diffraction on the Debye ring by using the 2nd Legendre Polynomial function, as given in (

(1).[35, 36]

$$P_2 = \frac{1}{2}\left(3 < cos^2\,\alpha > -1\right) \quad (1)$$

where $< cos^2 \alpha >$ is the average cosine squared value of the azimuthal angle θ, in a two dimensional azimuthal scan, and calculated from the measured intensity distributions using ((2)

$$< cos^2 \alpha >= \frac{\int_{-\frac{\pi}{2}}^{\frac{\pi}{2}} I(\alpha)\, cos^2 \alpha\, d\alpha}{\int_{-\frac{\pi}{2}}^{\frac{\pi}{2}} I(\alpha)\, d\alpha} \qquad (2)$$

where $I(\alpha)$ is the scattered intensity at α along the diffraction profile. The measured $I(\alpha)$ value was taken from the obtained XRD scatter curve, and directly put into a built Excel spreadsheet, to calculate $< cos^2 \alpha >$ and P_2 by using the (1 and (2 shown above. The integrals in ((2) were carried out for a fixed value of 2θ.

2.6 Testing of mechanical properties

Tensile tests of the silk composite fibres were carried out on an Instron 5565 universal test machine equipped with a 10 kN calibrated load cell at room temperature. The gauge length was 20 mm, and the cross-head speed in the direction parallel to the fibre array was 2 mm min^{-1}. The results obtained from the tensile tests were averaged over at least 3 measurements. The tensile Young's Modulus Ec (in the initial linear strain range of 0.0050-0.0100) was measured from the stress-strain curves.

Three-point bending flexural tests were performed on the coagulated silk film (as it was too brittle to be gripped for a tensile test) using the same machine equipped with a bending fixture and a 10 kN calibrated load cell. A cross-head speed of 2 mm min^{-1} was used. The flexural modulus at the maximum stress was calculated from the stress-strain curves, and was calculated at the outer surface of the test specimen at mid-span.

3. RESULTS AND DISCUSSION

3.1 Microstructure of ASCs

Cross-sectional optical images of the ASC structures processed for different dissolution times, at 30 °C are presented in Figure 3. It can be seen that a single unprocessed silk fibre contains several hundred filaments, and forms a loose microstructure with significant inner space. It is likely that the unprocessed fibres can swell in the epoxy resin as they are not bound together with any coagulated silk matrix. As the dissolution progresses, there was a trend that the overall cross-sectional size of the final silk composite was gradually decreased (as the proportion of matrix phase increased). Interestingly, the gaps between each individual filament were decreased (Figure 3a-c), and eventually a tightly compacted lenticular shape of a silk composite fibre bundle emerged after 2 h (Figure 3d). Figure 3e-h indicates that the amount of the inner core fibre filaments continuously reduced with time. The dissolved fibre turning into matrix appears in the outer layer of fibre core and surrounding at each of filaments to form a close packing silk composite. This transition in morphology is also shown in the series of samples made at 40 °C, seen in Figure S2, while the interfacial bonding of ASCs processed under 60 °C for one hour is shown in Figure S3.

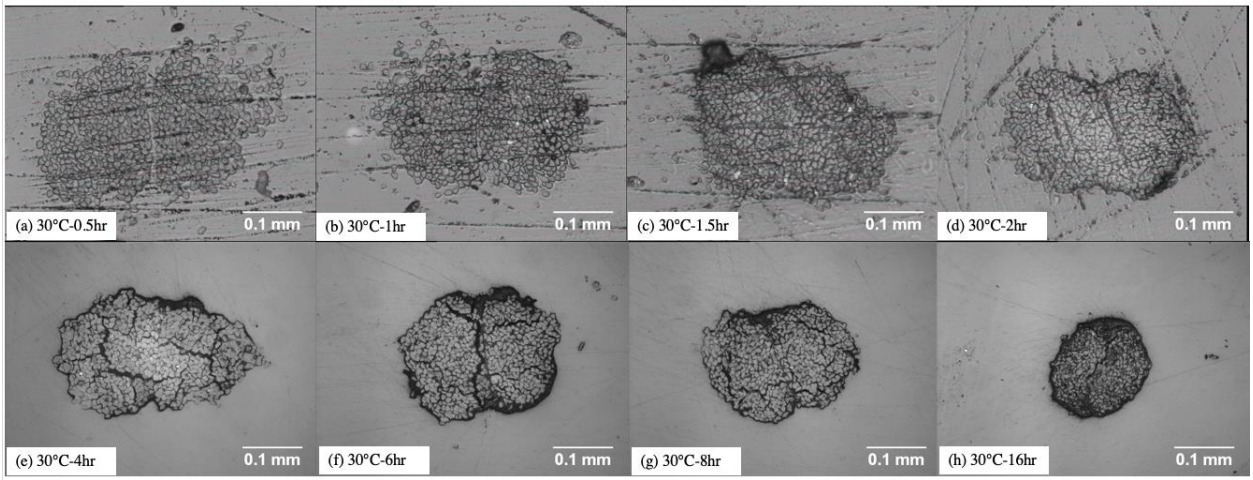

Figure 3 Microscopy cross-sectional images of single partial dissolved silk fibre threads, processed under 30 °C, for different length of time, and observed at x 200 magnification.

It can be proposed that in the early dissolution stage (up to 2 h) the IL infiltrates in-between each filament. In these early dissolution times, the outer layer of each individual filament is dissolved and forms a silk matrix.

Eventually once all the inner space is filled and a close packed structure is formed, it becomes more difficult for the IL to penetrate through. As seen in Figure 4, the size of silk filaments appear smaller in the outer layer of fibre core compared with inner core filaments, a clear halo of silk matrix is observed. It can therefore be proposed that as dissolution proceeds, the IL dissolves the exposed outer layers of the fibre, forming a well adhered silk fibre core and an outer halo of silk matrix.

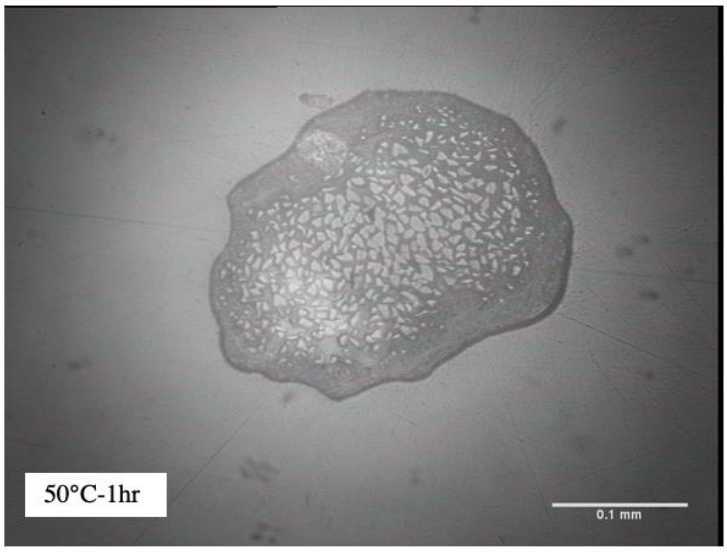

Figure 4 Optical microscope image of silk fibre processed under 50 °C for 1 hour, observed under x 200 magnification.

3.2 Characterization of single ASC/coagulated film orientation

Figure 5a shows a typical XRD 2θ diffraction profiles of a raw silk fibre, a partially dissolved fibre (50 °C for 1 hour) and the coagulated silk film from [C2mim][OAc] solution with 5 wt. % silk fibre. Theoretically, the dissolution process applied on the raw silk fibre could change the resultant crystalline structure, particularly for the CSF (the matrix phase). However, the 2θ scans showed that the position of the three most obvious crystalline diffraction peaks (9.8°, 20.6° and 29°) were all present for the samples at the different dissolution stages. Most importantly, the diffraction curve of the raw silk fibre was very similar to the partially dissolved fibre curve, with only a small reduction in the intensity of the highest diffraction peak. For this reason it was concluded that the change in the crystalline structure could not be used to follow and measure the dissolution fraction in these silk fibre composites, as we have previously used for single cotton composites, so a different approach was required.[37] The XRD azimuthal scans for the same three

samples, illustrated a much more significant change in the intensity distribution, see Figure 5b. This is related to a large difference between the highly aligned crystalline orientation of the raw silk fibres and the randomly oriented crystals in the CSF (matrix phase). The three collected azimuthal scans were normalized to give the same total area under the curves.

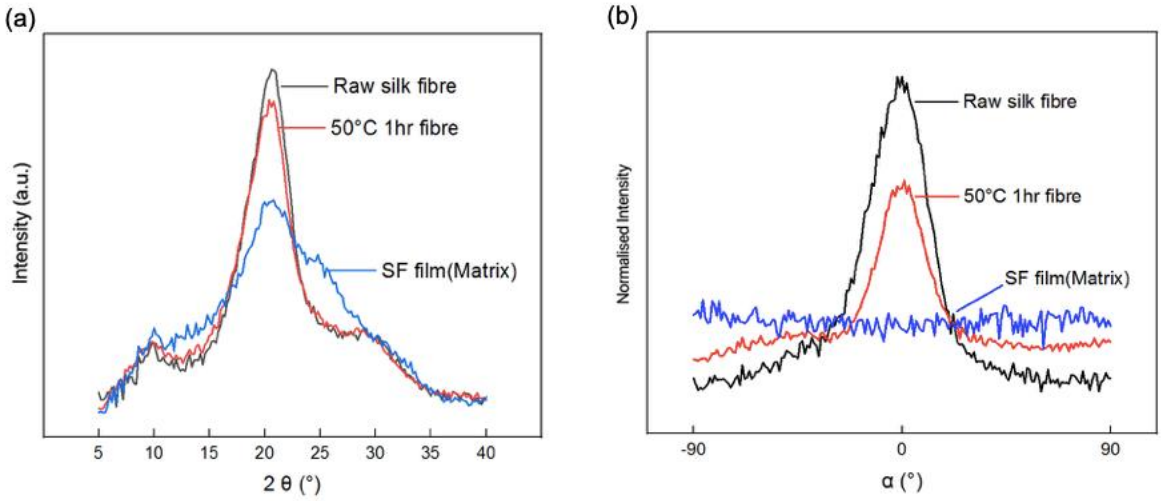

Figure 5 Comparison of WAXD diffraction profiles of raw silk fibre, partially dissolved fibre, and coagulated silk fibroin film, at (a) 2θ scan, (b) azimuthal scan.

As mentioned above in section 2.5, an XRD azimuthal scan was carried out by fixing 2θ at the angle with the highest crystalline diffraction peak (20.6°), and then scanning through azimuthal angles from -90° to 90°. At this 2θ position, there was only one crystalline peak in the diffraction curve located at $\alpha = 0°$. Our proposal is that the average orientation of each silk composite fibre is a sum of the preferred crystalline orientation in the unprocessed silk fibre and the randomly oriented coagulated silk film. For the silk composite fibres, the normalized peak height was seen to fall which was directly related to the percentage of crystalline regions being dissolved by the IL and being transformed into a randomly oriented crystalline structure after coagulation, increasing

the height of this second component. Interestingly, as shown in Figure 6, the full width half height (FWHH) of the central silk reflection at $\alpha = 0°$, was found to remain constant as the dissolution progressed, suggesting strongly that, the undissolved portion of each silk filament is unaffected by the dissolution process.

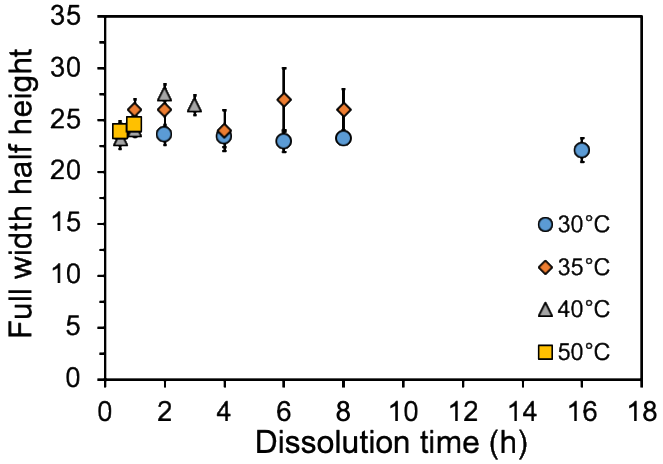

Figure 6 Full width half height of XRD azimuthal scan diffraction curves at different times and processing temperatures. The legend shows the temperatures at which the samples were processed.

Figure 5b indicates that the raw silk fibre shows the highest peak intensity, whereas the coagulated silk film shows a constant intensity distribution throughout the whole scanning angle, confirming random crystalline orientation. Compared to the raw silk fibre, the normalised peak intensity of the partially dissolved silk fibre is lower while its baseline (from the CSF component) is higher, caused by the dissolution process transforming the silk fibres into a randomly oriented coagulated silk fraction whose intensity is therefore independent of α.

Accordingly, the average P_2 value of each partially dissolved silk fibre composite obtained from processing at various times and temperatures, could be calculated from the distribution curve by using ((1), and these results are shown in Figure 7A. Theoretically, the P_2 value should be equal to 0.25 for a random 2D distribution, and equal to 1 for a perfect alignment. As the randomly oriented component increased in the composite this would result in a fall in the average P_2 value. As expected, composites processed under longer dissolution times or higher dissolution temperatures, were measured to have a lower P_2 value, as shown in Figure 7A. For ASC processed in [C2mim][OAc] at various times and temperatures, a broadly linear reduction of the average P_2 value was seen. For this reason, similar average P_2 values could be achieved at different reaction temperatures, with a shorter dissolution time needed when the temperature was increased. It can be assumed that [C2mim][OAc] continuously and effectively dissolves the silk fibres to gradually generate more coagulated silk fraction (randomly oriented crystal structure) in the composite.

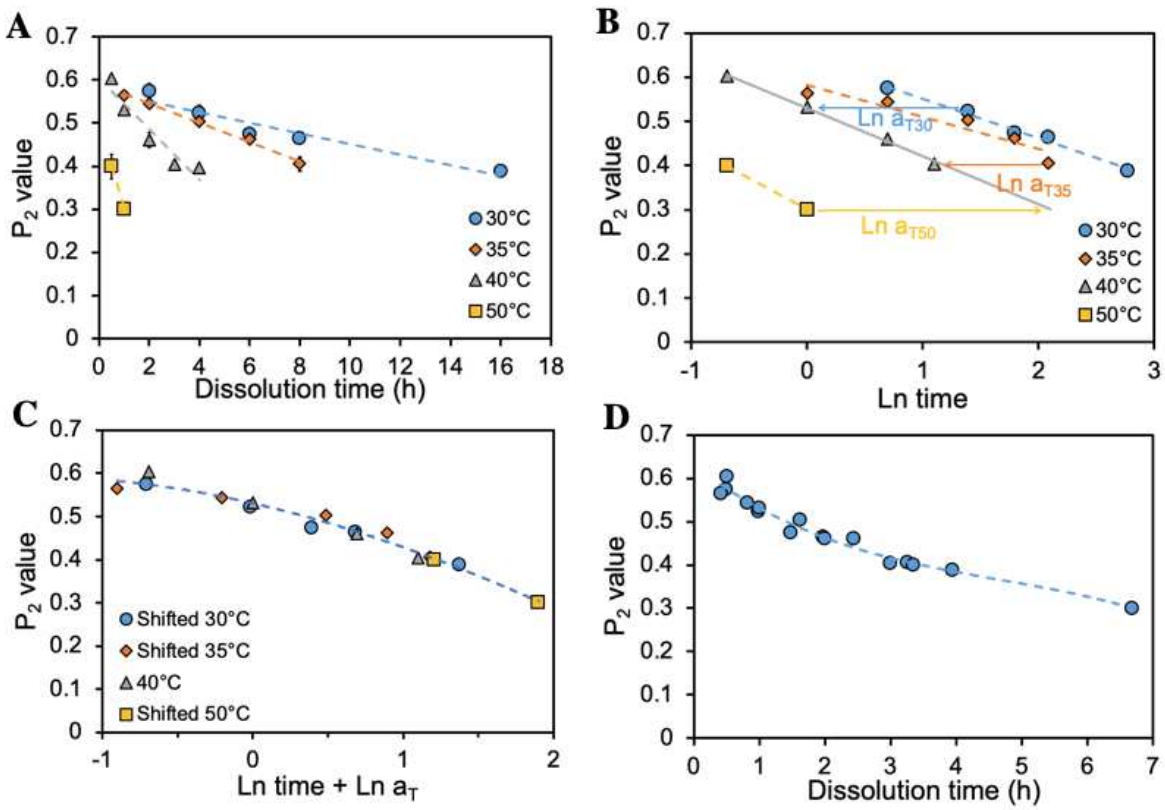

Figure 7 Averaged P_2 values calculated from XRD azimuthal scans for single ASC being dissolved in [C2mim][OAc] at various times and temperatures (A); A graph to show details of shift method, by using 40 °C as reference temperature (B); Shifted P_2 value of single ASC, generated as a master curve in ln space (C); Master curve for P_2 value of single ASC with respect to dissolution time, at a reference temperature 40 °C (D).

The average P_2 values measured from the silk fibre composites (Figure 7A) showed that the dissolution process occurred more rapidly at higher temperatures. It is proposed that the relationship between dissolution time and temperature could be combined into one curve ("master curve") using the concept of time-temperature superposition, which has been used extensively in polymer rheology measurements. A similar approach was recently proposed by this group in the

study of the dissolution of flax fibres in [C2mim][OAc].[38] From this previous work, the idea is to examine the data as a function of the logarithm of time (ln time) and superimpose the various temperature curves in ln time. A simple multiplicative factor (a_T) could thus relate the temperature and time results, via (3 and (4.

$$t_R = t_1 a_T \quad (3)$$

$$\ln t_R = \ln t_1 + \ln a_T \quad (4)$$

where T_1 is the temperature, T_R is reference temperature, t_1, t_R is the time before and after scaling respectively and ln a_T is the shift factor in ln time. The master curve could thus be constructed by simultaneously shifting different temperature curves horizontally along the logarithm of dissolution time axis, to achieve the best possible overlap. Figure 7B illustrates schematically the construction of the master curve, which involved a number of steps to generate the best master curve by using the middle temperature (40 °C -grey data points) as the reference T_R data set (in ln time), allowing the line to be extended to give further guidance. Then the other temperature curves were shifted along the X axis (ln time) towards the reference set to make them overlap, with the horizontal shift called the shift factor (ln a_T). Next, a second polynomial was fitted to the obtained superimposed data sets, and then the individual shift factors were varied to maximise the R^2 value, so as to provide the best fit between this polynomial and the shifted points. Figure 7C shows this final master curve for the variation of the average P_2 value with ln time shifted to 40 °C.

It is more useful to plot the average P_2 value with respect to the linear dissolution time for the silk fibres dissolving in [C2mim][OAc], as shown in Figure 7D. It can be expected that completely

dissolving the silk fibre could be achieved by a 7 h dissolution time at 40 °C, as its P_2 value approached that of the randomly oriented silk film, i.e. 0.25.

We can now plot the shift factors ($\ln a_T$) versus the inverse of temperature, as shown in Figure 8. This plot is linear and indicates that the dissolution process follows an Arrhenius like behaviour, i.e. ((5 and (6).[39]

$$a_T = Ae^{-\frac{Ea}{RT}} \quad (5)$$

$$\ln a_T = \ln A - \frac{Ea}{RT} \quad (6)$$

where E_a is the Arrhenius activation energy, R is the gas constant and T the temperature. The dissolution activation energy of the silk fibre in [C2mim][OAc] was therefore calculated at 138 ± 13 kJ/mol.

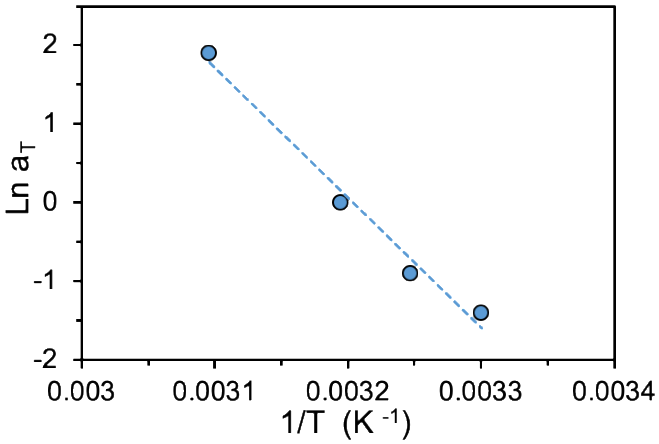

Figure 8 P_2 shift factors ($\ln a_T$) as a function of inverse temperature, indicating Arrhenius behaviour.

3.3 Measurement of the volume fraction of the coagulated silk matrix (V_m) in the all silk composites

As the dissolution process breaks hydrogen bonds and disulfide bonds in the crystalline regions of the silk fibre, the preferentially oriented crystalline structure is transformed into a randomly oriented coagulated fraction. This was seen from the XRD azimuthal scans, where the average P_2 value was seen to fall as the dissolution reaction progresses, suggesting the amount of ordered crystalline structure being dissolved increases. The P_2 value of the two individual components, of the composites, fibre and matrix, were measured to be 0.62 (P_2 fibre) from the unprocessed raw silk fibre and 0.25 (P_2 matrix) from the coagulated silk film. We then propose that the coagulated matrix fraction (V_m) of each partially dissolved silk composite, can be quantitatively determined from the measured average P_2 value, by assuming a linear mixing rule as expressed in ((7 and (8).

$$P_2{}^{composite} = P_2{}^{fibre} V_{fibre} + P_2{}^{matrix} V_{matrix} \quad (7)$$

Rearranging (7 , to make V_m the subject leads to

$$V_m = \frac{P_2{}^{fibre} - P_2{}^{composite}}{P_2{}^{fibre} - P_2{}^{matrix}} \quad (8)$$

Assuming $V_{fibre} + V_m = 1$

Therefore, the value of the dissolved and coagulated matrix fraction, V_m, for ASC obtained under various dissolution temperature as a function of dissolution time can be calculated and this is shown in Figure 9A. As expected, longer dissolution times generated more of the randomly oriented matrix phase and consequently lead to a reduction of the remaining silk fibre fraction and an associated large V_m. These results agreed with the previous cross-sectional optical microscope

images (Figure 3), showing that the amount of the remaining silk fibre filaments reduced with the dissolution time, and the matrix amount correspondingly increased.

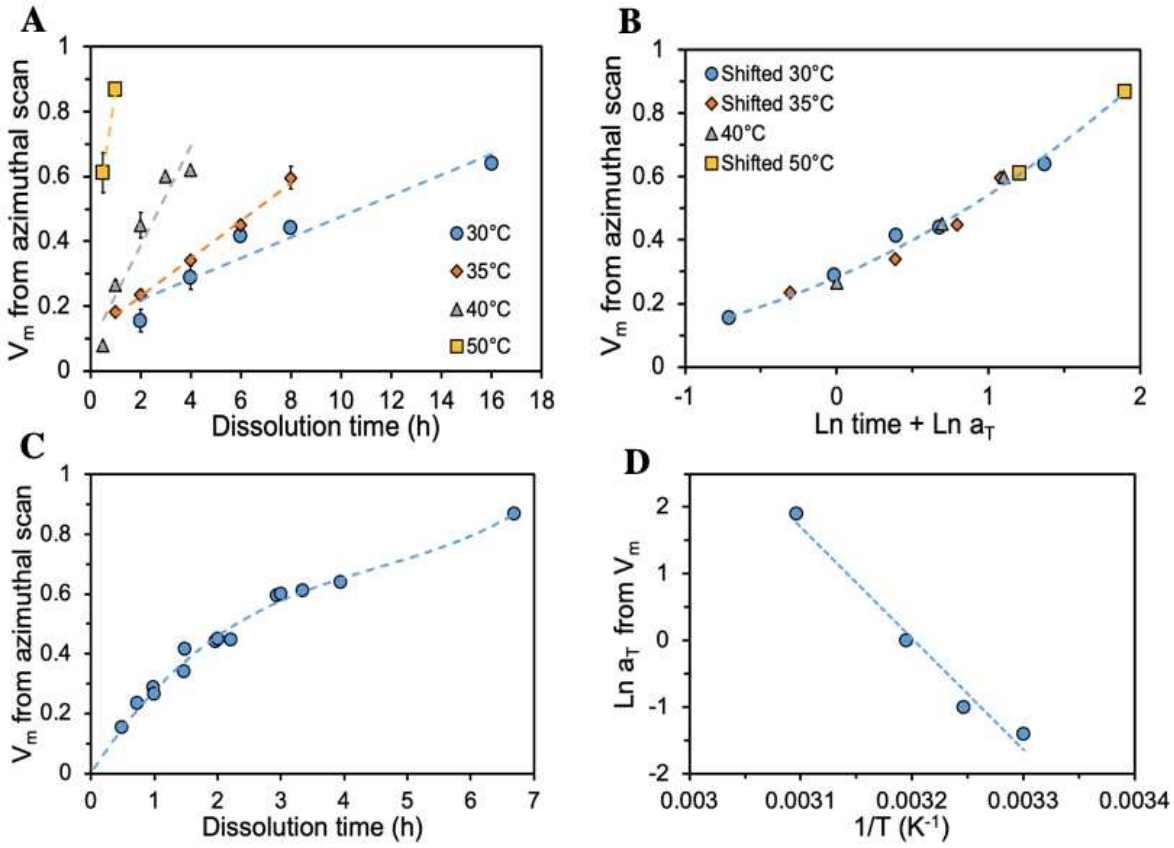

Figure 9 Single ASC volume of matrix measured from difference in P_2 value (A); Master curves of Shifted V_m value of ASC in ln space (B), V_m value of single ASC with respect to dissolution time, at a reference temperature 40 °C (C); V_m shift factors (ln a_T) as a function of inverse temperature, indicating Arrhenius behaviour (D).

As demonstrated above, the silk fibre dissolution process displays time temperature superposition, so the V_m should likewise obey TTS. In Figure 9B, a shifted master curve of the V_m

values of the obtained ASCs was constructed by using the same shifting method, as introduced above, again using 40 °C as the reference temperature.

After all the data points from different temperatures were shifted, the complete master curve in dissolution time was obtained, and is shown in Figure 9C. This curve showed the change in the matrix fraction, V_m, of the silk composites dissolving in [C2mim][OAc] with respect to dissolution time, at a reference temperature 40 °C. In the first two hours, the [C2mim][OAc] dissolved up to 50 % of fibre. However, in the second stage 2 to 4 hours only a further 20 % of silk fibres were dissolved, which indicates that the dissolution rate has slowed down. However, from the shifted master curve, the dissolution process still follows the time-temperature superposition principle.

These shift factors, from the V_m TTS shifting, can now be plotted as a function of inverse temperature as before for the P_2 results. A straight line is again found to fit the data points, reflecting Arrhenius behaviour, as shown in Figure 9D. From these V_m measurements, the dissolution of silk fibre in [C2mim][OAc] was calculated to have an activation energy of 139 ± 15 kJ/ mol. This is very similar to the value obtained from the P_2 TTS analysis and is a confirmation of the validity of our procedure.

3.4 Mechanical properties of single ASC

Figure 10 shows the results of Young's Modulus measurements carried out on composite fibres formed at a temperature of 30 °C for times up to 16 hours. It would be expected, from a simple parallel rule of mixtures that the Young's Modulus of each processed single ASCs would

continuously decrease, due to the amount of the reinforcing fibre reducing. However, as shown in Figure 10, the measured modulus values gradually increase at the early stages of the dissolution, reaching a maximum at around 2 hours and then afterwards decreases.

As we mentioned previously when discussing the optical micrographs of the raw and partially dissolved fibres, the specific fibre structure resulted in significant interior space in between each filament. At an early dissolution stage, we suggest that the created matrix is not sufficient to fill up all the gaps between filaments. The results of this would be that there is not good stress transfer between all the filaments (insufficient matrix) resulting in a lower measured modulus. Similar observations were reported by Soykeabkaew et al.[40] in all cellulose composites. Furthermore, they observed that after two hours of immersion time, sufficient amount of the outer layer of fibres were dissolved to create a matrix phase to bond the remaining fibre cores. This could also explain why the experimental Young's Modulus value of a raw undissolved fibre was only 6.17 GPa, which was close to the value of those at early stages of the dissolution (0.5, 1 hour at 30 °C).

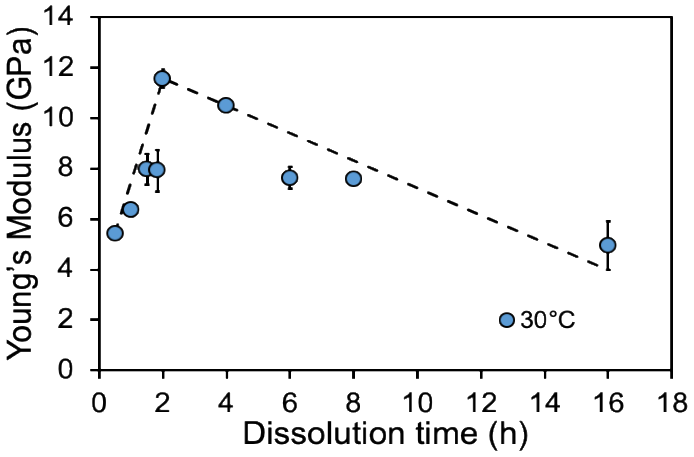

Figure 10 Modulus value of single ASC dissolved for different length of time, at 30 °C, the dashed line is guide for the eye, and not a fit to the data.

Consequently, combined with previous silk fibre microstructure results, the dissolution procedure of a single silk fibre can be proposed by the schematic diagram, shown in Figure 11. In the early stage, [C2mim][OAc] can infiltrate in between each filament of raw silk fibre (Figure 11a), transforming dissolved fibre into matrix to provide a close packing fibre microstructure (Figure 11b), which we name the 'preformed stage'. At two hours (30 °C), all the internal space is filled and the measured Young's modulus reaches a peak. Following this, more silk fibres are dissolved forming as an outer ring on the preformed fibre core (Figure 11c). As more matrix is generated the thicker this ring becomes, eventually a completely dissolved film matrix would be formed (Figure 11d). We could propose that to form a composite from a single fibre, then the optimum dissolved volume fraction (~20 %) would occur at two hours at 30 °C. However, to make a composite with multiple fibres, more matrix phase would be required to combine all the various fibres into a homogeneous composite (this is normally around 30-40 % for a typical composite or in this case around 1 hour at 40 °C).

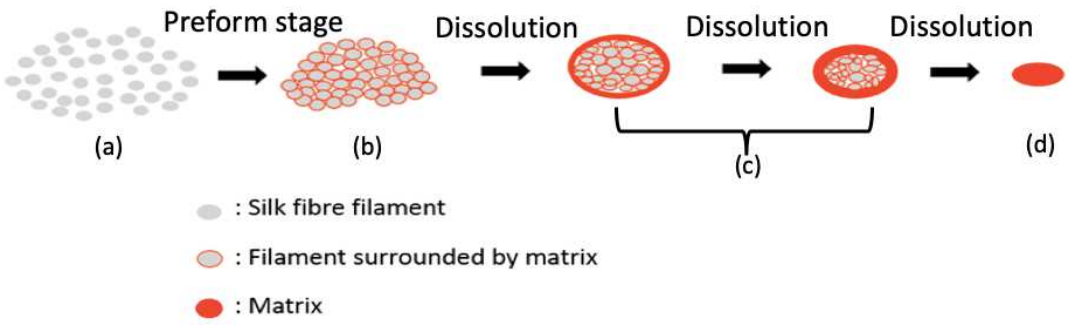

Figure 11 Schematic representation of silk fibre dissolution procedure, dissolution starts from (a) undissolved raw silk fibre, to (b) ASC with close packing microstructure, (c) ASCs with different amount of matrix, and (d) completely dissolved film matrix.

The Young's Modulus value of single ASCs obtained from various dissolution temperatures are summarized in Figure 12A, after removing the results before the preformed stage. It demonstrates a trend that the experimentally measured Young's Modulus continuously decreases, and does so more rapidly at higher temperature.

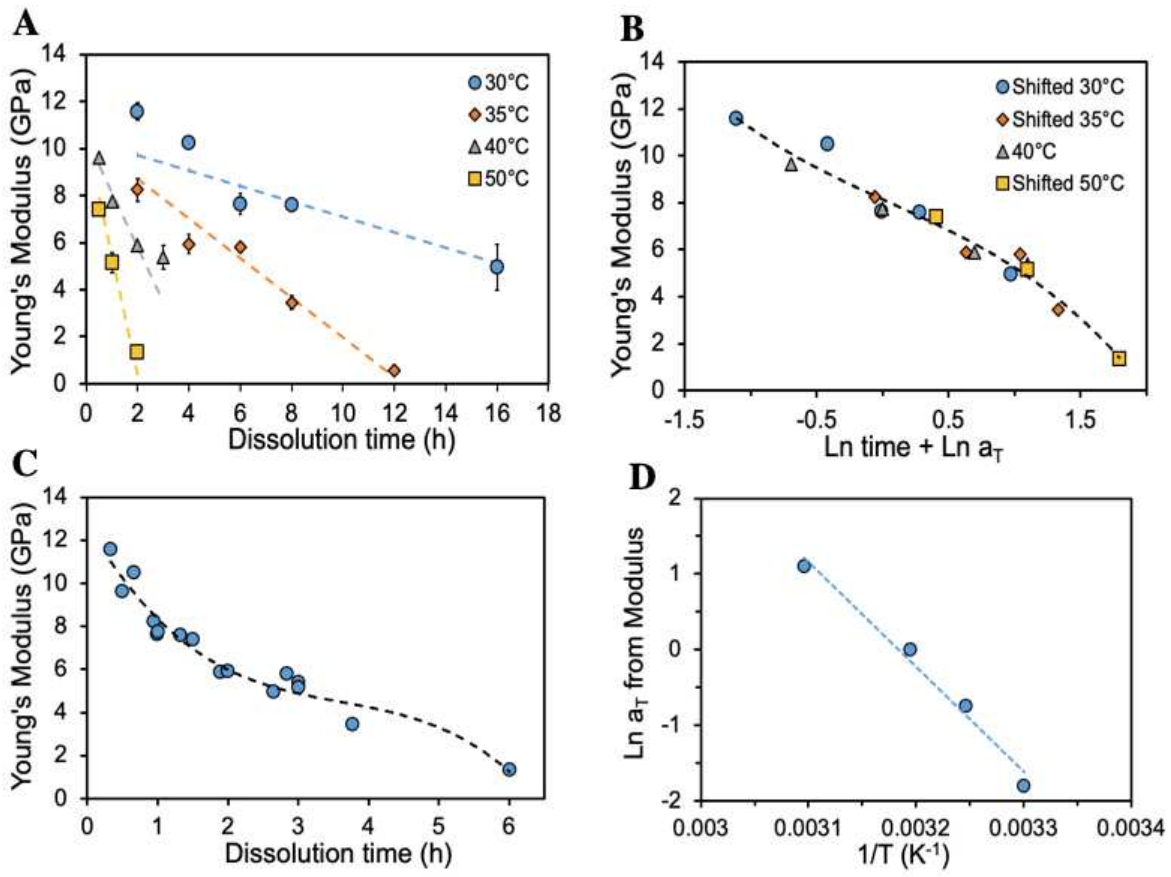

Figure 12 Young's Modulus change of each processed single ASC at various dissolution time (A); Master curves of Shifted Young's Modulus value of ASC in ln space (B); each processed single ASC as a function of dissolution time, at a reference temperature 40 °C, the intercept of this curve gives unprocessed silk fibre Young's Modulus to be 12.74 GPa (C); Young's Modulus shift factors (ln a_T) as a function of inverse temperature, indicating Arrhenius behaviour (D).

We now see if the variation of the modulus measurements also obey the time-temperature superposition principle. Figure 12B shows the results of using the same shifting procedure as described above, again using 40 °C as the reference temperature. These results indicate that the

modulus curves at different temperatures were related to one another by certain shift factors (Ln a_T). Interestingly, in terms of composite production, the same modulus value could be obtained by either increasing the dissolution temperature or increasing the dissolution time. After all of the individual data points were shifted, the complete TTS curve of single ASCs Young's Modulus values (in dissolution time) is shown in Figure 12C, based on a 40 °C reference temperature.

These results mirror the shape of the matrix fraction master curve (Figure 9C) as this is the main controlling factor in determine the composite modulus. Figure 9C shows that the matrix fraction initially rises quickly with the dissolution time, leading to the rapidly decreasing modulus shown in Figure 12C. As the matrix dissolution rate slows (when all the interior spaces in the silk multi-filaments are filled), then the fall in Young's Modulus also slows down as shown in Figure 12C. Figure 12D shows that relationship between the shifting factors and inverse temperature is once again Arrhenius, being linear when the shift factors are plotted against 1/T.

The dissolution activation energy from Figure 12D was measured to be 116 ± 12 kJ/mol. This is similar to the two values obtained from the P_2 and V_m time temperature shifting. A comparison of the three measured dissolution activation energy results can be seen in Figure 13. The average value was calculated to be 131 ± 8 kJ/mol. To the best of our knowledge the activation energy for dissolving silk fibroin hasn't previously been reported, but here we can compare it to the viscosity activation energies of silk fibroin in [BMIM]Ac, 71.9 kJ/mol, across the temperature range 25-45 °C studied by Susanin et al.[41], and 50-60 kJ/mol at 70-100 °C in [BMIM]Cl reported by Yao et al.[42] It is also of interest to compare the value of [C2mim][OAc] viscosity activation energy of 40

kJ/mol[43], and 65 kJ/mol for 10 w/w% of cellulose in [C2mim][OAc].[44] More recently reported is the enthalpy of solvation at -96.4 kJ/mol for cellulose in [C2mim][OAc].[45]

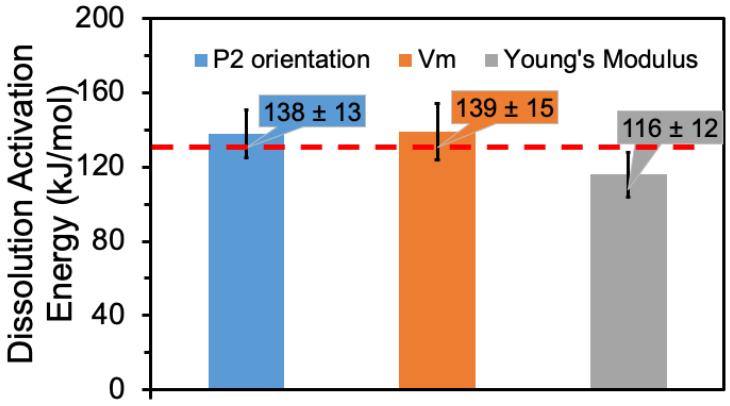

Figure 13 A graph to summarise the dissolution activation energy measured through three different methods, horizontal dashed line indicates the average value, which goes through all measurements within their error bars.

After acquiring the Young's Modulus values of each processed single ASCs, it is of final interest to see how these correlate with the matrix fraction V_m obtained from the XRD azimuthal scan, in particular to assess the applicability of the well-known rule of mixtures (ROM) in our fibre composite and to quantify the effect of reinforced fibre volume on the resulted mechanical behaviour.

Therefore, the Young's Modulus master curve values of each ASCs (in Figure 12C) was plotted as a function of the corresponding V_m master curve values from the azimuthal scan (in Figure 9C) and is shown in Figure 14. Based on the parallel and series rules of mixture models[46], Voigt

(parallel and upper bound) and Reuss (series and lower bound) predictions were used to estimate the effective modulus in the composite. Plotting the ROM model boundary curves requires the two limiting moduli values, i.e. from the ordered raw silk undissolved fibre and the coagulated silk matrix from the prepared film. Extrapolation of the modulus TTS curve (Figure 12C) gives the raw preformed well-aligned silk fibre modulus value as 12.7 ± 1.3 GPa ($V_m = 0$). The three-point bending experiment measured on the coagulated silk film gave a value of 1.0 ± 0.4 GPa ($V_m = 1$).

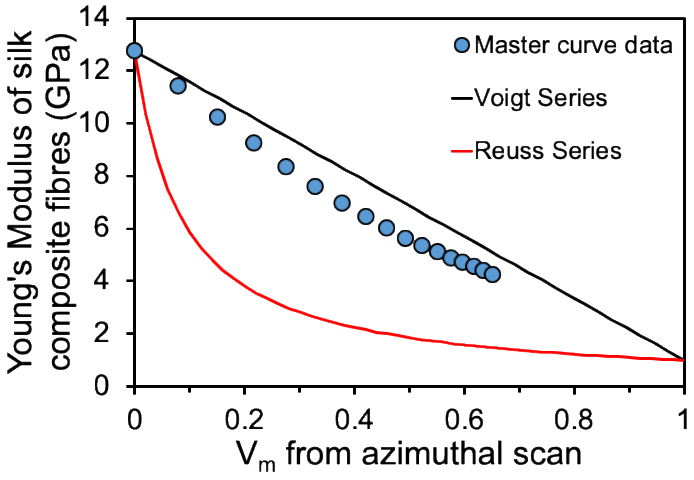

Figure 14 Rule of mixture curve for single silk composite fibres Young's Modulus as a function of corresponding V_m, with Voigt and Reuss boundary lines to indicate the rule of mixture theory.

The Voigt model assumes that the strain of the fibre is equal to the strain of matrix (parallel model), while the Reuss series proposes that the stress of fibre was equal to the stress of matrix.[47] It could be observed that all the master curves data points, as expected, lie between the two boundary curves. The results are close to the Voigt rule of mixtures, up to a matrix fraction (V_m) of ~70 %, which is a normal location for most fibre reinforced composite materials.

4. Conclusions

In this article we report for the first time the use of time-temperature-superposition to follow the dissolution of silk by a solvent, enabling a dissolution activation energy to be quantified. We employed a novel method to do this, tracking the change in orientation through XRD azimuthal scans. The focus of this study was to investigate the dissolution dynamics of silk fibres in 1-ethyl-3-methylimidazolium acetate ([C2mim][OAc]) and the structure and properties of the resulting composites. The single silk composite fibres were prepared by the surface selective dissolution method. [C2mim][OAc] was chosen as the solvent and methanol as the anti-solvent. The dissolution process was carried out under various times and temperatures allowing a range of the partially dissolved silk composite fibres to be created. By using optical microscopy, it was found that silk composite fibre is composed of original undissolved silk filaments surrounded by a coagulated silk matrix phase. The tensile Young's Modulus of each silk composite filament was measured, and it was found that initially the modulus value increased linearly to a peak (11.6 ± 0.4 GPa at time 2h) and then declined linearly thereafter with time. By combining the results from optical microscopy and Young's Modulus testing, a preform stage was identified, in which the [C2mim][OAc] infiltrates in between each multi-filament, transforming dissolved fibre into matrix to provide a tightly packed fibre core microstructure.

In an XRD azimuthal scan, a substantial change was measured in the intensity distribution curves of raw silk fibres and the randomly oriented coagulated silk matrix, as shown in Figure 5b For the silk composite fibres, we found that the average value of P_2 is directly related to the fraction of the

original silk fibres and the fraction of the coagulated matrix (randomly oriented structure). The average crystalline orientation of the resulted silk composite fibres was therefore measured by analyzing the azimuthal scan diffraction curves and calculating the 2nd Legendre Polynomial function (P_2 value). Importantly, the construction of the master curve of the measured P_2 values vs time required only the application of a horizontal shift upon reference data set, which results in a single smooth curve across all temperature sets. The shift factors (Ln a_T) were found to follow Arrhenius behaviour with a calculated activation energy of 138 ± 13 kJ/mol. Using a simple rule of mixtures, the dissolved silk matrix volume fraction (V_m) was determined from the calculated average P_2 values. It was found that these results could also be shifted to a single master curve with a very similar activation energy of 139 ± 15 kJ/ mol. The same shifting method was also applied to construct Young's Modulus master curves, giving a resultant activation energy of 116 ± 12 kJ/mol. The dissolution activation energy measured for the three different methods were found to agree with each other within the errors, giving an average value of 131 ± 8 kJ/mol. Finally, the plot of Young's Modulus master curve results of each silk composite filament vs the silk matrix volume fraction master curve results were observed to lie between Voigt and Reuss boundary curves, although much closer to the upper Voigt bound, which represents an iso-strain condition in the silk composite fibres.

ASSOCIATED CONTENT

Supporting Information

Figure S1-S3 X-ray 2D scan photos of raw silk fibre and coagulated silk film; Microscopy cross-sectional images of single partial dissolved silk fibre threads processed under 40 °C, for different length of time, and observed at x 200 magnification; Scanning electron micrographs of single

partial dissolved silk fibre, processed under 60 °C for one hour, observed at x 1000, x2000, x4000 magnification, from left to right.

AUTHOR INFORMATION

Corresponding Author

*E-mail address: M.E.Ries@leeds.ac.uk

ACKNOWLEDGMENT

The authors are greatly thankful to James Hawkins, Maer Alanazi, and Dr Daniel Baker in Soft Matter Group from School of Physics and Astronomy for experimental help. The authors express their appreciation to Yunhao Liang for kindly providing the steaming method to make SF film.

Data can be found at https://doi.org/10.5518/894

REFERENCES

1. Yallew, T. B.; Aregawi, S.; Kumar, P.; Singh, I., Response of natural fiber reinforced polymer composites when subjected to various environments. *Int. J. Plast. Technol.* **2018,** *22* (1), 56-72.
2. Pickering, K. L.; Efendy, M. G. A.; Le, T. M., A review of recent developments in natural fibre composites and their mechanical performance. *Compos. Pt. A-Appl. Sci. Manuf.* **2016,** *83*, 98-112.
3. Thyavihalli Girijappa, Y. G.; Mavinkere Rangappa, S.; Parameswaranpillai, J.; Siengchin, S., Natural Fibers as Sustainable and Renewable Resource for Development of Eco-Friendly Composites: A Comprehensive Review. *Frontiers in Materials* **2019,** *6*.
4. Vollrath, F.; Porter, D., Silks as ancient models for modern polymers. *Polymer* **2009,** *50* (24), 5623-5632.
5. Melke, J.; Midha, S.; Ghosh, S.; Ito, K.; Hofmann, S., Silk fibroin as biomaterial for bone tissue engineering. *Acta Biomater.* **2016,** *31*, 1-16.
6. Cheung, H. Y.; Lau, K. T., Mechanical performance of silk-based structural composites. *Key Eng. Mater.* **2006,** *326-328*, 457-460.

7. Chen, F.; Porter, D.; Vollrath, F., Silk cocoon (Bombyx mori): Multi-layer structure and mechanical properties. *Acta Biomater.* **2012,** *8* (7), 2620-2627.
8. Moy, R. L.; Lee, A.; Zalka, A., COMMONLY USED SUTURE MATERIALS IN SKIN SURGERY. *Am. Fam. Physician* **1991,** *44* (6), 2123-2128.
9. Kaplan, D.; Adams, W. W.; Farmer, B.; Viney, C., SILK - BIOLOGY, STRUCTURE, PROPERTIES, AND GENETICS. In *Silk Polymers: Materials Science and Biotechnology*, Kaplan, D.; Adams, W. W.; Farmer, B.; Viney, C., Eds. Amer Chemical Soc: Washington, 1994; Vol. 544, pp 2-16.
10. Altman, G. H.; Diaz, F.; Jakuba, C.; Calabro, T.; Horan, R. L.; Chen, J. S.; Lu, H.; Richmond, J.; Kaplan, D. L., Silk-based biomaterials. *Biomaterials* **2003,** *24* (3), 401-416.
11. Vepari, C.; Kaplan, D. L., Silk as a biomaterial. *Prog. Polym. Sci.* **2007,** *32* (8-9), 991-1007.
12. Kundu, B.; Rajkhowa, R.; Kundu, S. C.; Wang, X. G., Silk fibroin biomaterials for tissue regenerations. *Adv. Drug Delivery Rev.* **2013,** *65* (4), 457-470.
13. Nguyen, T. P.; Nguyen, Q. V.; Nguyen, V. H.; Le, T. H.; Huynh, V. Q. N.; Vo, D. V. N.; Trinh, Q. T.; Kim, S. Y.; Le, Q. V., Silk Fibroin-Based Biomaterials for Biomedical Applications: A Review. *Polymers* **2019,** *11* (12), 25.
14. Nazarov, R.; Jin, H. J.; Kaplan, D. L., Porous 3-D scaffolds from regenerated silk fibroin. *Biomacromolecules* **2004,** *5* (3), 718-726.
15. Tamada, Y., New process to form a silk fibroin porous 3-D structure. *Biomacromolecules* **2005,** *6* (6), 3100-3106.
16. Ramamoorthy, S. K.; Skrifvars, M.; Persson, A., A Review of Natural Fibers Used in Biocomposites: Plant, Animal and Regenerated Cellulose Fibers. *Polym. Rev.* **2015,** *55* (1), 107-162.
17. Belhaj Khalifa, I.; Ladhari, N.; Touay, M., Application of sericin to modify textile supports. *J. Text. Inst.* **2012,** *103* (4), 370-377.
18. Zhou, C. Z.; Confalonieri, F.; Medina, N.; Zivanovic, Y.; Esnault, C.; Yang, T.; Jacquet, M.; Janin, J.; Duguet, M.; Perasso, R.; Li, Z. G., Fine organization of Bombyx mori fibroin heavy chain gene. *Nucleic Acids Res.* **2000,** *28* (12), 2413-9.
19. Suzuki, Y.; Aoki, A.; Nakazawa, Y.; Knight, D. P.; Asakura, T., Structural Analysis of the Synthetic Peptide (Ala-Gly-Ser-Gly-Ala-Gly)(5), a Model for the Crystalline Domain of Bombyx mori Silk Fibroin, Studied with C-13 CP/MAS NMR, REDOR, and Statistical Mechanical Calculations. *Macromolecules* **2010,** *43* (22), 9434-9440.
20. Crowhurst, L.; Mawdsley, P. R.; Perez-Arlandis, J. M.; Salter, P. A.; Welton, T., Solvent–solute interactions in ionic liquids. *Phys. Chem. Chem. Phys.* **2003,** *5* (13), 2790-2794.
21. Dupont, J.; de Souza, R. F.; Suarez, P. A. Z., Ionic liquid (molten salt) phase organometallic catalysis. *Chem. Rev.* **2002,** *102* (10), 3667-3691.
22. Earle, M. J.; Esperanca, J.; Gilea, M. A.; Lopes, J. N. C.; Rebelo, L. P. N.; Magee, J. W.; Seddon, K. R.; Widegren, J. A., The distillation and volatility of ionic liquids. *Nature* **2006,** *439* (7078), 831-834.
23. Fort, D. A.; Remsing, R. C.; Swatloski, R. P.; Moyna, P.; Moyna, G.; Rogers, R. D., Can ionic liquids dissolve wood? Processing and analysis of lignocellulosic materials with 1-n-butyl-3-methylimidazolium chloride. *Green Chem.* **2007,** *9* (1), 63-69.
24. El Seoud, O. A.; Koschella, A.; Fidale, L. C.; Dorn, S.; Heinze, T., Applications of ionic liquids in carbohydrate chemistry: A window of opportunities. *Biomacromolecules* **2007,** *8* (9), 2629-2647.

25. Mantz, R. A.; Fox, D. M.; Green, J. M.; Fylstra, P. A.; De Long, H. C.; Trulove, P. C., Dissolution of Biopolymers using ionic liquids. *Z. Naturforsch., A: Phys. Sci.* **2007,** *62* (5-6), 275-280.
26. Swatloski, R. P.; Spear, S. K.; Holbrey, J. D.; Rogers, R. D., Dissolution of cellose with ionic liquids. *J. Am. Chem. Soc.* **2002,** *124* (18), 4974-4975.
27. Phillips, D. M.; Drummy, L. F.; Conrady, D. G.; Fox, D. M.; Naik, R. R.; Stone, M. O.; Trulove, P. C.; De Long, H. C.; Mantz, R. A., Dissolution and regeneration of Bombyx mori Silk fibroin using ionic liquids. *J. Am. Chem. Soc.* **2004,** *126* (44), 14350-14351.
28. Stanton, J.; Xue, Y.; Pandher, P.; Malek, L.; Brown, T.; Hu, X.; Salas-de la Cruz, D., Impact of ionic liquid type on the structure, morphology and properties of silk-cellulose biocomposite materials. *Int. J. Biol. Macromol.* **2018,** *108*, 333-341.
29. Skarmoutsos, I.; Dellis, D.; Matthews, R. P.; Welton, T.; Hunt, P. A., Hydrogen Bonding in 1-Butyl- and 1-Ethyl-3-methylimidazolium Chloride Ionic Liquids. *J. Phys. Chem. B* **2012,** *116* (16), 4921-4933.
30. Wang, H.; Gurau, G.; Rogers, R. D., Dissolution of Biomass Using Ionic Liquids. In *Structures and Interactions of Ionic Liquids*, Zhang, S.; Wang, J.; Lu, X.; Zhou, Q., Eds. 2014; Vol. 151, pp 79-105.
31. Chen, X.; Shao, Z. Z.; Knight, D. P.; Vollrath, F., Conformation transition kinetics of Bombyx mori silk protein. *Proteins: Struct., Funct., Bioinf.* **2007,** *68* (1), 223-231.
32. Chen, X.; Knight, D. P.; Shao, Z., β-turn formation during the conformation transition in silk fibroin. *Soft Matter* **2009,** *5* (14), 2777-2781.
33. Chen, J.; Vongsanga, K.; Wang, X.; Byrne, N., What Happens during Natural Protein Fibre Dissolution in Ionic Liquids. *Materials* **2014,** *7* (9), 6158-6168.
34. Hamidi, Y. K.; Yalcinkaya, M. A.; Guloglu, G. E.; Pishvar, M.; Amirkhosravi, M.; Altan, M. C., Silk as a Natural Reinforcement: Processing and Properties of Silk/Epoxy Composite Laminates. *Materials* **2018,** *11* (11), 2135.
35. Hermans, J. J.; Hermans, P. H.; Vermaas, D.; Weidinger, A., QUANTITATIVE EVALUATION OF ORIENTATION IN CELLULOSE FIBRES FROM THE X-RAY FIBRE DIAGRAM. *Recl. Trav. Chim. Pays-Bas* **1946,** *65* (7-8), 427-447.
36. White, J. L.; Spruiell, J. E., THE SPECIFICATION OF ORIENTATION AND ITS DEVELOPMENT IN POLYMER PROCESSING. *Polym. Eng. Sci.* **1983,** *23* (5), 247-256.
37. Liang, Y. H.; Hawkins, J. E.; Ries, M. E.; Hine, P. J., Dissolution of cotton by 1-ethyl-3-methylimidazolium acetate studied with time-temperature superposition for three different fibre arrangements. *Cellulose*, in press.
38. Hawkins, J. E., Yunhao Liang, M.E. Ries, P.J. Hine, Time Temperature Superposition of the Dissolution of Flax Fibres by the Ionic Liquid 1-ethyl-3-methylimidazolium acetate with cosolvent Dimethyl Sulfoxide. *Carbohydrate Polymer Technologies and Applications* **2021,** *2*, 100021.
39. Laidler, K. J., THE DEVELOPMENT OF THE ARRHENIUS EQUATION. *J. Chem. Educ.* **1984,** *61* (6), 494-498.
40. Soykeabkaew, N.; Arimoto, N.; Nishino, T.; Peijs, T., All-cellulose composites by surface selective dissolution of aligned ligno-cellulosic fibres. *Compos. Sci. Technol.* **2008,** *68* (10-11), 2201-2207.
41. Susanin, A. I.; Sashina, E. S.; Novoselov, N. P.; Zaborkskii, M., STUDY OF THE RHEOLOGICAL CHARACTERISTICS OF SOLUTIONS OF SILK FIBROIN IN 1-BUTYL-3-

METHYLIMIDAZOLIUM ACETATE AND FILMS BASED ON THEM. *Fibre Chem.* **2017,** *49* (2), 88-96.
42. Yao, Y. B.; Mukuze, K. S.; Zhang, Y. M.; Wang, H. P., Rheological behavior of cellulose/silk fibroin blend solutions with ionic liquid as solvent. *Cellulose* **2014,** *21* (1), 675-684.
43. Green, S. M.; Ries, M. E.; Moffat, J.; Budtova, T., NMR and Rheological Study of Anion Size Influence on the Properties of Two Imidazoliumbased Ionic Liquids. *Sci Rep* **2017,** *7*, 12.
44. Sescousse, R.; Le, K. A.; Ries, M. E.; Budtova, T., Viscosity of Cellulose-Imidazolium-Based Ionic Liquid Solutions. *J. Phys. Chem. B* **2010,** *114* (21), 7222-7228.
45. Brehm, M.; Pulst, M.; Kressler, J.; Sebastiani, D., Triazolium-Based Ionic Liquids: A Novel Class of Cellulose Solvents. *J. Phys. Chem. B* **2019,** *123* (18), 3994-4003.
46. Bower, D. I., *An Introduction to Polymer Physics*. Cambridge University Press: Cambridge, 2002.
47. Kim, H. S., On the rule of mixtures for the hardness of particle reinforced composites. *Mater. Sci. Eng., A* **2000,** *289* (1-2), 30-33.

For Table of Contents Only